J. Fluid Mech. (2008), *vol.* 614, *pp.* 495–507.
doi:10.1017/S0022112008003741 Printed in the United Kingdom

On the rate of spatial predictability in near-wall turbulence

NIKOLAY NIKITIN

Institute of Mechanics, Moscow State University, 1 Michurinsky Prospect, 119899 Moscow, Russia

(Received 17 April 2008 and in revised form 28 July 2008)

Spatial evolution of small perturbations introduced into an inlet cross-section of fully developed turbulent flow in a long straight circular pipe is investigated via direct numerical simulation (DNS). The turbulent inflow field is extracted from an auxiliary streamwise-periodic simulation running in parallel with the main spatial simulation. It is shown that mean perturbation amplitude $\overline{\varepsilon}$ increases exponentially with distance downstream. The growth rate is found to be constant when normalized by viscous length, $\overline{\varepsilon} \sim \exp(0.0021x^+)$ over the considered Reynolds-number range $140 \leqslant Re_\tau \leqslant 320$. The universal character of perturbation growth is confirmed by channel-flow simulations.

1. Introduction

Consider a streamwise-homogeneous turbulent fluid flow in a long straight duct of, say, a circular cross-section. The introduction of a small velocity perturbation into a fixed cross-section causes flow modification downstream. The goal of the present work is to estimate the rate of predictability of the instantaneous structure of the turbulent flow by analysing the velocity difference between the flows with and without perturbations.

Instability and unpredictability may be considered as essential parts of the definition of turbulence. In contrast to the averaged characteristics which are fairly predictable, the difference between the instantaneous velocity fields of two turbulent flows will grow until saturated at the level comparable to the level of turbulent fluctuations no matter how small it might be initially. Considerable theoretical and experimental effort has been devoted to tackling the problem of turbulence predictability. The first analytical and computational studies (Lorenz 1963; Smagorinsky 1969; Kraichnan 1970; Leith 1971; Leith & Kraichnan 1972; Lilly 1972; Orszag & Patterson 1972) dealt with homogeneous isotropic turbulence in the context of meteorological applications. In the cited papers, the underlying measure of unpredictability is the growth in the difference between the Eulerian velocity fields of pairs of flows chosen from statistically identical ensembles: $\delta\boldsymbol{u}(\boldsymbol{x}, t) = \boldsymbol{u}^{(1)}(\boldsymbol{x}, t) - \boldsymbol{u}^{(2)}(\boldsymbol{x}, t)$. In order to investigate the behaviour of $\delta\boldsymbol{u}$ when it is small, we must generalize the hydrodynamic stability theory, which was very fruitful in the context of laminar to turbulent transition, to circumstances where the unperturbed base flow is a complicated function of space and time. An interesting application of the analysis of $\delta\boldsymbol{u}$ behaviour in direct numerical simulations of a turbulent channel flow is given in the work of Keefe, Moin & Kim (1992) where it was used to calculate the Lyapunov dimension of the turbulent attractor.

Studies in which the equations of motion were linearized about the turbulent mean velocity field span a considerable period of time. As a result, it is now well established, for example, that the dominant mechanism of turbulence production in free turbulent shear flow is the inviscid inflectional instability of the turbulent mean-velocity profile (Gaster, Kit & Wygnanski 1985). One of the latest approaches (Chernyshenko & Baig 2005; del Álamo & Jimenez 2006) based on non-modal growth of perturbations of the mean velocity profile was shown to have a significant predictive ability for the organized structures in near-wall turbulent flow. However, only constant-in-time viscosity (laminar in Chernyshenko & Baig 2005; turbulent in del Álamo & Jimenez 2006) was accounted for in those works. Taking time-dependent Reynolds stresses into account with the help of empirical turbulence models gives controversial results. Eigensolutions of the extended Orr–Sommerfeld equation with different turbulence closure models were compared with experimental results of organized disturbance evolution in fully developed turbulent channel and boundary-layer flows. Hussain & Reynolds (1970, 1972) and Reynolds & Hussain (1972) gave damped oscillations whereas Sen and colleagues (see for references Sen & Veeravalli 2000*a*) report a range of unstable modes. An agreement with experiment was claimed in both cases. The difference is due to the difference in turbulence models. The first direct numerical simulation (DNS) based measurement of the complete mean response of a turbulent channel flow to small external disturbances was described by Luchini, Quadrio & Zuccher (2006). Space–time impulsive perturbations were applied at one channel wall, and the linear response describing their mean effect on the flow field as a function of spatial and temporal separations was estimated. It was shown that the turbulent response differs from the response of a laminar flow with the turbulent mean velocity profile as the base flow.

Analytic investigation of the behaviour of small perturbations of turbulent flow is extremely difficult, even within a linearized approach, owing to the high complexity of the unperturbed flow. Direct experimental quantification of the stability properties of turbulent flows is also difficult since it implies a comparison of two realizations of fluid motion which differ initially by a small perturbation field. Hussain & Reynolds (1970), Hussain & Reynolds (1972) and Sen & Veeravalli (2000*b*) measured the evolution of controlled disturbances. Numerical simulations offer more suitable investigation tools for these purposes. Velocity perturbation of any spatial and temporal structure can be imposed onto the simulated turbulent flow. After that, two simulations, with and without perturbation, can be run in parallel providing data for the direct comparison and the analysis of the deviation between the flows.

One of the problems connected with DNS and LES of spatially developing flows is imposing turbulent inflow boundary conditions. In most cases, the flow downstream is highly dependent on the condition at the inlet, making it necessary to specify realistic time series of turbulent fluctuations that are in equilibrium with the mean flow. Perhaps the most straightforward approach to simulating spatially developing flow is to start far upstream with a laminar profile plus some random disturbances and then allow a natural transition to occur. This approach has been used in simulations focusing on the transitional process itself (Rai & Moin 1993; Nikitin 1995, 2001) and has the advantage that no turbulent fluctuations are required at the inlet. This method is not generally applicable to turbulent simulations, since simulating the transition process is in itself a costly procedure. A number of strategies for generating inflow boundary conditions have been proposed, and a comprehensive literature survey on this topic may be found in Lund, Wu & Squires (1998) and Druault *et al* (2005).

For the class of wall-bounded flows, the method where the inflow boundary condition is extracted from the auxiliary simulation with streamwise-periodic conditions is one of the most suitable. Let $\boldsymbol{u}_t(\boldsymbol{x}, t)$ be the velocity field in a streamwise-periodic turbulent solution of the Navier–Stokes equations with a given period l_x,

$$\boldsymbol{u}_t(x + l_x, y, z, t) \equiv \boldsymbol{u}_t(x, y, z, t). \tag{1.1}$$

Using the results of the auxiliary streamwise-periodic simulation for the main spatial simulation means that the two simulations can be run in parallel. The inflow boundary condition for the spatial simulation is extracted from a chosen cross-section of the streamwise-periodic simulation, say $x = 0$, at each time instant,

$$\boldsymbol{u}(0, y, z, t) = \boldsymbol{u}_t(0, y, z, t) \quad \forall\ y, z, t. \tag{1.2}$$

This method is especially suited to internal flows subjected to spatial non-uniformity of different kinds (see, for example, Kaltenbach 1993; Wagner & Friedrich 1994; Bae *et al* 2006; Yakhot, Liu & Nikitin 2006).

Using the turbulent inflow condition extracted from the auxiliary streamwise-periodic simulation is commonly considered as ideal since it provides a flow with correct statistics, phase information and dynamics. However, as was shown in Nikitin (2007), the memory of the inflow is evident in the spatially evolving flow over a considerable distance downstream. In particular, this may result in spatial periodicity of the flow.

The point of the Nikitin (2007) paper follows from the observation that in the case of geometry homogeneous in the x-direction, the streamwise-periodic solution

$$\boldsymbol{u}(x, y, z, t) = \boldsymbol{u}_t(x, y, z, t), \tag{1.3}$$

satisfies both the Navier–Stokes equations for $x \geqslant 0$ and the inflow boundary condition (1.2) and, thus, presents a solution of the spatially evolving flow problem. In a series of numerical simulations of turbulent pipe flow, it was shown that although the solution (1.3) is convectively unstable, the memory of the inflow boundary condition is evident over a significant distance from the inlet. In the cases considered, an almost periodic flow was established (with less than 1 % relative deviation from the periodicity) over a distance as large as 70 pipe radii.

This result shows that an inflow condition from an auxiliary streamwise-periodic simulation is not as ideal as is commonly assumed, since it causes a spatial periodicity which is not physical for turbulent flows. To enhance the departure from the periodicity, some kind of additional perturbation should be imposed on the inflow velocity. This perturbation should be small; otherwise, it may result in flow deviation from the fully developed turbulent state in terms of its mean (in time) values, and some distance downstream is required in order to recover the flow. Since the analysis in Nikitin (2007) was performed for only one geometry and one value of the Reynolds number, the influence of these parameters on the rate of perturbation growth and the rate of flow departure from the periodicity remains unknown. Thus, this knowledge, apart from its fundamental significance, is crucial for proper application of the highly popular method of imposing inflow boundary conditions in direct numerical simulations.

In the present paper, the procedure of a spatially evolving flow simulation adopted in Nikitin (2007), supplemented with the imposition of an artificial perturbation in the inlet cross-section, is used for the turbulent flow stability investigation. The main advantages of this model are twofold. First, the use of the inflow field from the auxiliary simulation provides the inflow data with correct turbulence statistics

and dynamics. Secondly the 'exact' solution for spatially evolving flow presented by the spatially periodic flow (1.3) can be used as a reference 'unperturbed' flow for analysing its stability characteristics. The majority of simulations were performed for the case of circular pipe flow in the Reynolds-number range $4000 \leqslant Re \leqslant 10\,000$ ($140 \leqslant Re_\tau \leqslant 320$). One simulation case for the plane channel flow was considered as well, in order to confirm the main result of the investigation.

2. Formulation and numerical method

We consider a flow of viscous incompressible fluid through a long circular pipe $0 \leqslant x < \infty$, $y^2 + z^2 \leqslant R^2$ driven by a given unsteady inflow velocity with a positive flow rate. The flow is governed by the Navier–Stokes and continuity equations,

$$\frac{\partial \boldsymbol{u}}{\partial t} + (\boldsymbol{u}\cdot\nabla)\boldsymbol{u} = -\frac{1}{\rho}\nabla p + \nu\nabla^2\boldsymbol{u}, \quad \nabla\cdot\boldsymbol{u} = 0. \tag{2.1}$$

with a no-slip boundary condition on the rigid wall. Initial $\boldsymbol{u}|_{t=0}$ and inflow $\boldsymbol{u}|_{x=0}$ velocity fields are extracted from an auxiliary turbulent flow simulation with streamwise-periodic conditions (1.1). The procedure of generating the streamwise-periodic solution $\boldsymbol{u}_t(\boldsymbol{x}, t)$ is standard for DNS of turbulent pipe flow. At first, the auxiliary simulation is run alone until a statistically steady state is achieved. The instantaneous velocity field at this time, which is referred to as $t = 0$, is taken as the initial condition for the main simulation,

$$\boldsymbol{u}(x, y, z, 0) = \boldsymbol{u}_t(x, y, z, 0), \quad 0 \leqslant x < \infty, \ y^2 + z^2 \leqslant R^2. \tag{2.2}$$

After that, the auxiliary simulation is run in parallel with the main simulation. At each time instant $t > 0$, the velocity distribution in the cross-sectional plane $x = 0$ of the auxiliary simulation is transferred into the inlet cross-section of the main simulation. In addition, a certain small-amplitude artificial perturbation $\delta\boldsymbol{u}(0, y, z, t)$ is introduced into the inlet,

$$\boldsymbol{u}(0, y, z, t) = \boldsymbol{u}_t(0, y, z, t) + \delta\boldsymbol{u}(0, y, z, t). \tag{2.3}$$

The auxiliary simulation is carried out with a constant-flow-rate condition. The artificial inlet perturbation is chosen from a set of zero-flow-rate velocity fields, thus ensuring a constant (in time) flow rate in the main simulation.

In the present paper, we are focused on the spatio-temporal evolution of the perturbation field, which is defined as the difference between the actual and unperturbed velocity fields, the latter being presented by the streamwise-periodic solution of the auxiliary simulation

$$\delta\boldsymbol{u}(x, y, z, t) = \boldsymbol{u}(x, y, z, t) - \boldsymbol{u}_t(x, y, z, t), \quad x \geqslant 0, \quad t > 0. \tag{2.4}$$

The intensity of perturbation is characterized by a mean-square amplitude $\varepsilon(x, t)$, defined as a cross-sectional average

$$\varepsilon^2(x, t) = \frac{1}{|S|}\int\int |\delta\boldsymbol{u}(x, y, z, t)|^2 \, \mathrm{d}S. \tag{2.5}$$

Here, S is the cross-sectional area.

The Navier–Stokes equations in a cylindrical coordinate system (x, r, θ) are solved using a second-order finite-difference discretization scheme in space and a third-order semi-implicit Runge–Kutta method in time. A detailed description of the numerical method is given in Nikitin (2006).

Several types of steady and unsteady inflow perturbation fields $\delta\boldsymbol{u}|_{x=0}$ were tested. No visible variations in qualitative and quantitative behaviour of the perturbation field at $x > 0$ have been detected except in the immediate vicinity of the inlet. This is predictable, taking into account the high degree of spatial and temporal irregularity in the oncoming turbulent flow. The results shown below have been obtained with a steady inflow perturbation in the form

$$(\delta u_x, \delta u_r, \delta u_\theta) = \alpha(0, 0, r^2(1-r^2)\sin\theta), \tag{2.6}$$

with α in the range $10^{-10} - 10^{-8}$. Hereinafter, u_x, u_r and u_θ are the axial, radial and circumferential velocity components; all quantities are presented in the non-dimensional form with the pipe radius R and the Poiseuille flow centreline velocity U_0 (which is twice the bulk velocity U_b) as the length and velocity scales. Alternative non-dimesionalization based on the friction velocity $u_\tau = \sqrt{(\tau_w/\rho)}$ and friction length $l_\tau = \nu/u_\tau$ (τ_w is the mean wall friction) is denoted as usual by a superscript $^+$.

The main simulation is conducted in the computational domain of a finite length, $0 \leqslant x \leqslant L_x$, which is several times longer than the period of the underlying periodic flow. Soft boundary conditions in the form

$$\frac{\partial u_x}{\partial x} = \frac{\partial u_r}{\partial x} = \frac{\partial u_\theta}{\partial x} = 0, \quad x = L_x, \tag{2.7}$$

are applied at the outlet cross-section. During the course of the present simulations, it was found that outflow boundary conditions

$$\frac{\partial^2 u_x}{\partial x^2} = \frac{\partial^3 u_r}{\partial x^3} = \frac{\partial^3 u_\theta}{\partial x^3} = 0, \quad x = L_x, \tag{2.8}$$

used in Nikitin (1995, 2001), occasionally produce points with negative axial velocity in the near-wall region of the outlet cross-section, which, in turn, can lead to the eventual destruction of the numerical solution. Boundary conditions in the form (2.7) are free of such a deficiency, although they generate a higher perturbation in the outlet cross-section as compared with the conditions (2.8). It is rather more important that perturbation caused by artificial outflow conditions does not propagate upstream as time increases, and that its intensity decreases rapidly with distance from the outlet.

In all cases, the main simulation is performed with the same time step and mesh sizes in all three directions as in the associated auxiliary simulation. Thus, the numbers of grid points in the radial and angle directions are the same in both simulations, whereas the number of grid points in the axial direction in the main simulation is L_x/l_x times that in the auxiliary simulation.

3. Results

3.1. *Re = 5300 case*

Spatially evolving turbulent flow in a circular pipe at Reynolds number $Re = 2U_bR/\nu = 5300$ with inflow condition (1.2) was investigated in Nikitin (2007). Auxiliary simulation was conducted with the period $l_x = 10$, the length of the computational domain in the main simulation was $L_x = 80$. Two initial velocity fields $\boldsymbol{u}|_{t=0}$ were considered, the spatially periodic field of the auxiliary simulation (2.2) and the laminar flow velocity distribution $(u_x, u_r, u_\theta) = (1-r^2, 0, 0)$. It was shown that after a certain transitional stage at $0 \leqslant t \leqslant t_0 \sim 5\times10^2$ the flow does not depend on the initial condition. It takes the form of a streamwise-periodic flow of the auxiliary simulation with superimposed spatially growing perturbation. On average, the perturbation

Run	A	B	C	D
l_x	10	20	10	10
L_x	80	80	40	40
Grid (auxiliary simulation)	$256 \times 64 \times 128$	$512 \times 64 \times 128$	$256 \times 64 \times 128$	$512 \times 64 \times 128$
Grid (main simulation)	$2048 \times 64 \times 128$	$2048 \times 64 \times 128$	$1024 \times 64 \times 128$	$2048 \times 64 \times 128$
α	10^{-10}	10^{-8}	10^{-8}	10^{-10}

TABLE 1. Runs with $Re = 5300$.

amplitude increases exponentially with distance from the inlet and this trend does not change with time. Such a behaviour corresponds to convective instability of the underlying streamwise-periodic turbulent flow. The mean perturbation amplitude

$$\overline{\varepsilon}(x) = \left[\frac{1}{T}\int_{t_0}^{t_0+T} \varepsilon^2(x,t)\,\mathrm{d}t\right]^{1/2}, \tag{3.1}$$

was obtained by time averaging over the interval $T = 300$. Except in the immediate vicinity of the inlet, $\overline{\varepsilon}(x)$ behaves exponentially, $\overline{\varepsilon}(x) \sim \exp(\sigma x)$. The growth rate was estimated as $\sigma \approx 0.36$ (More careful examination of the Nikitin (2007) data reveals that a better approximation for the growth rate is $\sigma = 0.38$.)

In the simulations of Nikitin (2007), no artificial perturbation was introduced into the inlet. The only source of perturbations at $x > 0$ were the round-off errors of calculations. Thus, the effect of artificial inflow perturbations was not investigated. Also, the dependence of the perturbation growth rate on the period of underlying periodic flow and on the length of the computational domain was not determined in that work. Since all these factors may affect the flow evolution, additional simulations at $Re = 5300$ were performed in the present study. The corresponding simulation parameters including the amplitude α of the inlet perturbation (2.6) are given in table 1. The computational mesh in runs A, B and C was the same as in Nikitin (2007) with grid spacing in the axial, radial and angle directions of 7.0, 0.7–4.6 and 0–8.8 wall units, respectively. As was shown in Nikitin (2006), this grid spacing is adequate for the accurate reproduction of the first- and second-order statistics of the flow at the considered Reynolds number.

Space–time evolution of the perturbation amplitude $\varepsilon(x,t)$ in run A is shown in figure 1(*a*). In this run, grid and computational-domain parameters were exactly the same as in Nikitin (2007), but artificial perturbation, (2.6), with the amplitude $\alpha = 10^{-10}$ was introduced into the inlet cross-section of the main simulation. As in Nikitin (2007), where no artificial perturbation was introduced into the flow, in the initial stage of flow development, the most visible perturbation is in the downstream section of the pipe caused by the artificial outlet conditions. The outflow perturbation is $\approx 10^{-2}$ in the exit cross-section and decays rapidly in the upstream direction. It is important that it does not spread further upstream with time. The inflow perturbations propagate gradually downstream. The most growing perturbation has an exponential trend $\varepsilon \sim \exp(0.38x)$ and propagates with a velocity of about 0.4. Faster (but less growing) perturbations propagate downstream with a velocity up to ≈ 0.7, the maximum velocity in the flow. (Infinite-propagation-velocity perturbations caused by pressure fluctuations and by viscosity, decrease very rapidly in space and therefore cannot be detected on the background of round-off errors.) At the later stages of flow evolution, $t \gtrsim 200$, the exponential growth of perturbations spreads

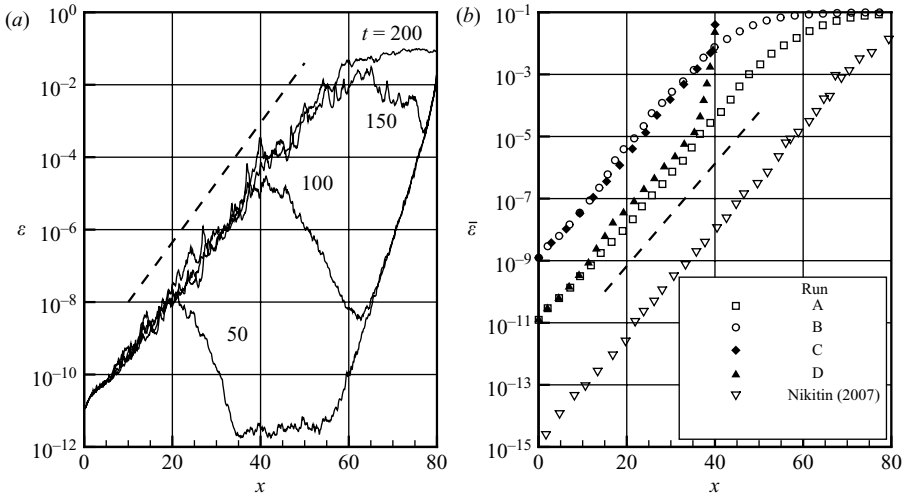

FIGURE 1. (*a*) Space–time evolution of perturbation amplitude, run A; (*b*) growth of mean perturbation amplitude at $Re = 5300$. - - -, $\sim\exp(0.38x)$.

downstream until finally saturating at the level of $\backsimeq 10^{-1}$, the amplitude of turbulent fluctuations in the flow.

The mean perturbation amplitude $\overline{\varepsilon}(x)$ defined in (3.1) was obtained by time-averaging over the interval $T = 500$ after the most growing perturbation reaches the exit cross-section at $t = t_0 = 200$. The graph of $\overline{\varepsilon}(x)$ is shown in figure 1(*b*) together with the corresponding graph from Nikitin (2007). The growth rates of small perturbations obtained in the two simulations agree very well, which demonstrates the independence of this quantity from the origin and the character of the flow perturbation.

The growth rate of small perturbations in a streamwise-periodic turbulent flow must be a varying function of the period length, $\sigma = \sigma(l_x)$. It may be expected, however, that the dependence of σ on l_x weakens at large l_x, approaching the value which characterizes the instability of a general turbulent flow at a given Reynolds number. To clarify this issue, simulation run B with longer period, $l_x = 20$, was performed. The number of grid points in the x-direction was doubled accordingly in the auxiliary simulation to keep the mesh spacings the same as in run A. Furthermore, the amplitude of the inlet perturbation was taken to be two orders higher than that in run A in the hope of obtaining nonlinear saturation of the perturbations at a smaller distance from the inlet. The resulting graph $\overline{\varepsilon}(x)$ for this run is presented in the figure 1(*b*). The same value, $\sigma \approx 0.38$, was obtained for the mean perturbation growth rate. The close values of the perturbation growth rate obtained for two different periods of underlying periodic flow is evidence that $\sigma \approx 0.38$ represents the instability rate of a general turbulent pipe flow at $Re = 5300$ rather than the instability rate of the periodic flow with some particular period.

The simulations presented so far were conducted with the same length of computational domain in the main simulation, $L_x = 80$. Taking into account the character of the evolution of the perturbation caused by the artificial outflow conditions (2.7), it is unlikely that evolution of the inflow perturbations can be seriously affected by the outflow. To be sure, additional runs C and D were performed with a different length of computational domain, $L_x = 40$. It was observed that the rate at which outflow perturbation decreases upstream depends on the axial grid

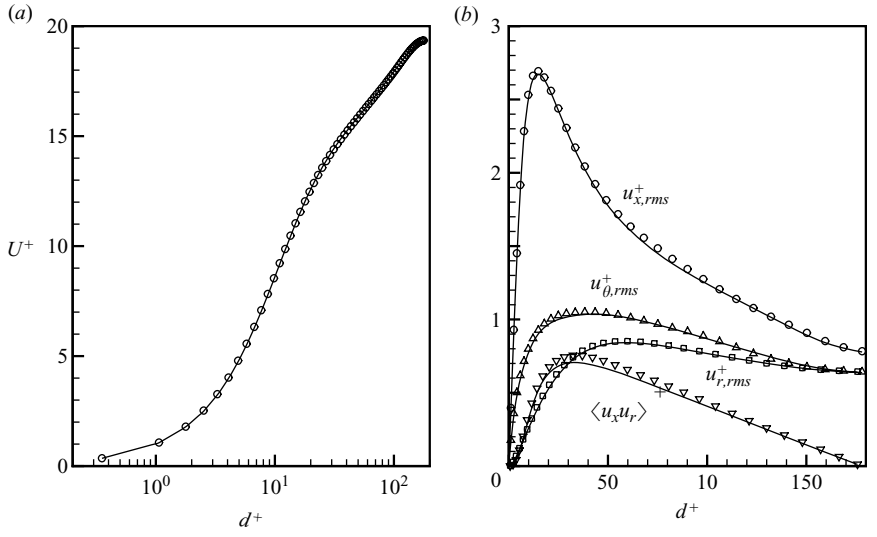

FIGURE 2. Flow statistics, run B. Lines, incoming flow; symbols, outgoing flow. (*a*) Mean velocity; (*b*) second-order statistics.

spacing. Therefore, one of the runs (run D) was performed with a finer grid in the streamwise direction. The results of these simulations are presented in figure 1(*b*). In both cases, the growth rate of small perturbations is close to $\sigma \approx 0.38$, proving the insignificance of the outflow effect.

The growth of perturbations means that the actual flow departs from the oncoming streamwise-periodic flow of the auxiliary simulation in terms of instantaneous velocity fields. It is important, however, that the two flows remain basically the same turbulent flow in terms of mean quantities. Mean velocity profile, r.m.s. values of the velocity fluctuations and Reynolds shear stress $\langle u_x u_r \rangle$ distribution in the end section of the pipe (run B) are shown in figure 2 and compared with the corresponding correlations in the oncoming flow. The presented quantities are given as functions of distance to the wall $d = 1 - r$. Mean quantities are obtained by averaging in time and in the azimuthal direction. The oncoming flow characteristics are averaged in the axial direction over the flow period, whereas the exit flow characteristics are averaged in the axial direction over the interval $70 \leqslant x \leqslant 80$. In this region, the difference between the instantaneous velocity fields in the actual and periodic flow have saturated on the level of turbulent fluctuations. However, as can be seen from figure 2, the two flows have almost exactly coincident mean characteristics.

The profiles of r.m.s. intensity of perturbation $\delta u_{rms}(x, r) = (\delta u^2_{x,rms} + \delta u^2_{r,rms} + \delta u^2_{\theta,rms})^{1/2}$ obtained in run B are shown in figure 3(*a*) for several x-stations as functions of the distance to the wall. Root mean square values are calculated by averaging in time and in the circumferential direction. At each station, the perturbation intensity is normalized, so that $\max \delta u_{rms} = 1$. The growing perturbation with a self-similar radial distribution of the r.m.s. intensity is formed soon after leaving the inlet cross-section and is held along the area of linear evolution. The shape of the r.m.s. intensity profile in this area is characterized by a distinct maximum at $d^+ \approx 13$ and a sharp reduction of perturbations at larger distances from the wall. Further downstream, when nonlinear effects became visible in perturbation evolution, the perturbations

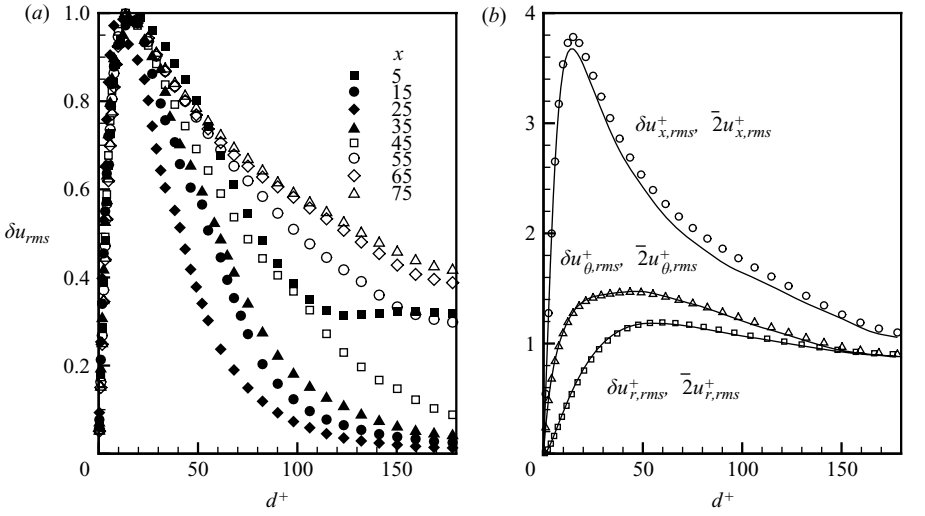

FIGURE 3. (*a*) Root mean square intensities of perturbations in several x-stations (run B); (*b*) three components of perturbation intensity at $x = 75$ compared with the three components of turbulent fluctuations multiplied by $\sqrt{2}$.

occupy a wider region from the wall and the fall in perturbation intensity with d is smoother.

Perturbation $\delta\boldsymbol{u}$ is defined as the velocity difference between the actual $\boldsymbol{u}$ and the unperturbed $\boldsymbol{u}_t$ flows. Taking into account that the mean velocity and the r.m.s. values in both flows are the same at each x-station, the following relation can be derived,

$$\delta u^2_{rms} = 2u^2_{rms} - 2\langle \boldsymbol{u}' \cdot \boldsymbol{u}'_t \rangle, \tag{3.2}$$

where $\boldsymbol{u}' = \boldsymbol{u} - \langle \boldsymbol{u} \rangle$ and $\boldsymbol{u}'_t = \boldsymbol{u}_t - \langle \boldsymbol{u}_t \rangle$ are turbulent fluctuations. Equation (3.2) shows that if the two flows are uncorrelated, then the r.m.s. amplitude of perturbation is $\sqrt{2}$ times the r.m.s. amplitude of turbulent fluctuations in each flow. Three components of perturbation intensity corresponding to the three velocity components in the last station, $x = 75$, are shown in figure 3(*b*). For comparison, r.m.s. intensities of velocity fluctuations multiplied by $\sqrt{2}$ are given in figure 3(*b*) as well. Close coincidence of the two profiles for each velocity component signifies that the perturbation growth in the flow eventually makes the flow uncorrelated with the underlying unperturbed flow.

3.2. *Other Reynolds numbers*

Similar simulations were conducted at two other Reynolds numbers, $Re = 4000$ (run E) and $Re = 10\,000$ (run F). The grid and flow parameters in these cases together with those in run A are given in table 2. In all cases, the mesh spacing was adequate for accurate representation of the main statistical characteristics.

It was expected that the rate of perturbation growth would be an increasing function of Reynolds number. The results of the simulations support this supposition. The resulting graphs $\overline{\varepsilon}(x)$ for different Reynolds numbers are presented in figure 4(*a*). In all cases, there is a distinct region of exponential growth in $\overline{\varepsilon}(x)$ with the growth rate increasing from $\sigma \approx 0.29$ at $Re = 4000$ to $\sigma \approx 0.71$ at $Re = 10\,000$.

In figure 4(*b*), the variation of $\overline{\varepsilon}$ with distance from the inlet is shown as a function of $x^+ \equiv xRe_\tau$, where $Re_\tau = u_\tau R/\nu$. In this representation, the graphs $\overline{\varepsilon}(x^+)$ remarkably, have the same growth rate $\sigma^+ = \sigma/Re_\tau$ in the range $0.0021 - 0.0022$ in all

Run	A	E	F	Channel flow
Re	5300	4000	10 000	5600
l_x	10	10	10	10
L_x	80	80	40	80
Re_τ	140	180	320	178
Grid (auxiliary simulation)	$256 \times 64 \times 128$	$256 \times 64 \times 128$	$256 \times 128 \times 256$	$256 \times 128 \times 64$
Grid (main simulation)	$2048 \times 64 \times 128$	$2048 \times 64 \times 128$	$1024 \times 128 \times 256$	$2048 \times 128 \times 64$
h_x^+	7.0	5.5	12.5	7.0
h_r^+	0.7–4.6	0.5–3.6	0.6–4.1	$h_y^+ = 0.9$–4.4
h_θ^+	0–8.8	0–6.9	0–7.9	$h_z^+ = 8.3$
α	10^{-10}	10^{-8}	2×10^{-10}	10^{-8}
σ	0.38	0.29	0.71	0.35
σ^+	0.0021	0.0021	0.0022	0.0020

TABLE 2. Grid and flow parameters.

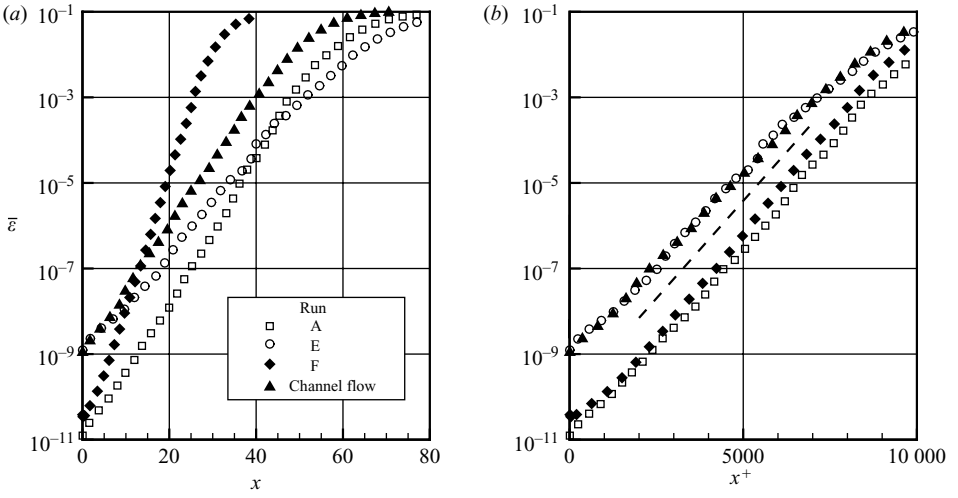

FIGURE 4. Growth of mean perturbation amplitude as function of (*a*) x and (*b*) x^+. - - -, $\sim\exp(0.0021x^+)$.

cases. The observation that the growth rate of small perturbations is constant when normalized by a friction length, suggests that instability of turbulent flow is a purely near-wall phenomenon with low dependence on the outer flow. In the linear stage of development, the profiles of perturbation intensities at all Reynolds numbers have a similar shape to those shown in figure 3(*a*). The maximal perturbation is observed at distance $d^+ \approx 13$ from the wall.

3.3. *Channel flow*

The near-wall character of instability in turbulent pipe flow suggests that instability with similar properties may be observed in other near-wall flows. To check the validity of this hypothesis, evolution of perturbations in plane channel flow was investigated following the procedure described in the previous sections for pipe flow. Simulation was performed at Reynolds number $2hU_b/\nu = 5600$ with a periodic condition in the spanwise direction z with a period $l_z = \pi$. The grid and flow parameters in the channel-flow simulation are given in table 2 (channel half-width h is a length scale).

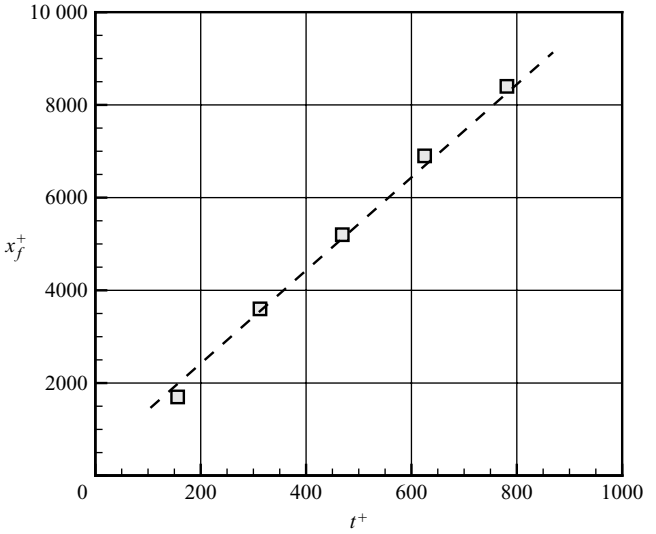

FIGURE 5. Propagation of the front edge of the most growing perturbation. Run A.

The inflow perturbation was taken in the form analogous to that in the pipe flow (2.6):

$$(\delta u_x, \delta u_y, \delta u_z) = \alpha(0, 0, y^2(1 - y^2)\sin(2\pi z/l_z)). \tag{3.3}$$

Spatial evolution of the mean perturbation amplitude is shown in figure 4. Perturbation growth rate $\sigma^+ \approx 0.002$ was obtained in channel flow. This is in reasonable agreement with the values $\sigma^+ \approx 0.0021 - 0.0022$ observed in pipe flow.

3.4. *Temporal evolution of perturbations*

As demonstrated in figure 1(*a*), the area occupied by the growing perturbation expands at the initial stage of flow evolution. Spatial growth of perturbations on this stage can be interpreted as a temporal growth with a simultaneous propagation downstream with a certain velocity. The propagation velocity of the most growing perturbation can be estimated my monitoring the position x_f of the front edge of the exponential part in the $\varepsilon(x, t)$ distribution. Although the front edge can be defined only within a certain tolerance, the graph $x_f^+(t^+)$ (shown in figure 5, run A) demonstrates a constant propagation velocity $C_f^+ = \mathrm{d}x_f^+/\mathrm{d}t^+ \approx 10$.

Another way to estimate propagation velocity follows from the supposition that the maximum amplification of perturbation takes place in a critical layer, where propagation velocity coincides with the velocity of a base flow. Since the maximum perturbation amplitude is at a distance $d^+ \approx 13$ from the wall where the mean velocity U^+ in the base turbulent flow is equal to 10, it is reasonable to expect that the propagation velocity of the most growing perturbation is also close to $C_f^+ = 10$.

The existence of near-wall structures in turbulent flows propagating with a velocity of about $10u_\tau$ is well known (e.g. see Morrison, Bullock & Kronauer 1971; Kim & Hussain 1993). There is no doubt that near-wall turbulent structures are closely connected to the growing perturbations investigated in the present work.

Spatial growth of perturbations can be interpreted as temporal growth in a moving frame of reference translating downstream with the propagation velocity C_f. Given the rate of spatial growth σ and the velocity of spatial propagation C_f, the rate of

temporal growth λ can be found as $\lambda = C_f \sigma$. Thus, for the values obtained in the present work, we can estimate $\lambda^+ \approx 0.021$.

The obtained rate of temporal growth agrees well with the results of Keefe *et al.* (1992). They estimated the dimension of the turbulent attractor underlying plane channel flow at very low Reynolds number $Re_\tau = 80$ and calculated Lyapunov spectra. Lyapunov exponents were calculated using two time steps $\Delta t u_\tau / h = 0.003$ and $\Delta t u_\tau / h = 0.0015$. The highest Lyapunov exponent, which characterizes the growth rate of the most growing small perturbation, was estimated as $\lambda_1 h / u_\tau \approx 1.4$ for the larger time step and $\lambda_1 h / u_\tau \approx 1.6$ for the smaller one. When normalized by viscous scales, these values give $\lambda_1^+ \approx 0.0175$ and $\lambda_1^+ \approx 0.02$, respectively.

4. Summary

Spatial growth of small perturbations introduced into the fully developed turbulent flow in a circular pipe and a plane channel was investigated by numerical simulations. Turbulent inflow velocity field was obtained in an auxiliary simulation with periodic conditions in the streamwise direction. The evolution of perturbation is analysed by comparing the flows with and without perturbations. The unperturbed flow is presented by the streamwise-periodic flow of the auxiliary simulation.

It was shown that the growth rate of the fastest-growing perturbation does not depend on the source of perturbation and the period of the underlying periodic flow. It was also shown that artificial outflow conditions, the length of computational domain and the grid spacing in the streamwise direction have a negligible effect on the perturbation growth rate.

The main result of the paper consists in the observation that the growth rate of the fastest-growing perturbation is a universal constant when normalized by wall units, $\sigma^+ \approx 0.0021$. This conclusion was derived from the analysis of a circular pipe flow in the Reynolds-number range $140 \leqslant Re_\tau \leqslant 320$ and plane channel flow at $Re_\tau = 178$.

The propagation velocity and the rate of temporal growth of the most growing perturbation was estimated as $C_f^+ \approx 10$ and $\lambda^+ \approx 0.021$. The latter is in very good agreement with the higher Liapunov exponent of the turbulent attractor obtained in Keefe *et al.* (1992).

The author is grateful to Professor S. Chernyshenko for the stimulating discussions and for his helpful comments on a draft of this manuscript. The research was started during the author's visit to the School of Engineering Sciences, University of Southampton, UK, which was supported by EPSRC under grant EP/D050871/1. The work was supported also by the Russian Foundation for Basic Research under grant 08-01-00489-a.

REFERENCES

Del Álamo, J. & Jimenez, J. 2006 Linear energy amplification in turbulent channels. *J. Fluid Mech.* **559**, 205–213.

Bae, J. H., Yoo, J. Y., Choi, H. & McEligot, D. M. 2006 Effects of large density variation on strongly heated internal air flows. *Phys. Fluids* **18**, 075102.

Chernyshenko, S. I. & Baig, M. F. 2005 The mechanism of streak formation in near-wall turbulence. *J. Fluid Mech.* **544**, 99–131.

Druault, Ph., Largeau, J. F., Coiffet, F., Delville, J., Bonnet, J. P. & Lardeau, S. 2005 Numerical investigation of turbulent inflow condition generation for LES. *Trans. ASME* I: *J. Fluids Engng* **127**, 945–948.

Gaster, M., Kit, E. & Wygnanski, I. 1985 Large-scale structures in a forced turbulent mixing layer. *J. Fluid Mech.* **150**, 23–39.

Hussain, A. K. M. F. & Reynolds, W. C. 1970 The mechanism of an organized wave in turbulent shear flow. *J. Fluid Mech.* **41**, 241–258.

Hussain, A. K. M. F. & Reynolds, W. C. 1972 The mechanism of an organized wave in turbulent shear flow. Part 2. Experimental results. *J. Fluid Mech.* **54**, 241–261.

Kaltenbach, H.-J. 1993 Large eddy simulation of flow in a plane, asymmetric diffuser. *Annual Research Briefs–1993, Center for Turbulence Research* 101.

Keefe, L., Moin, P. & Kim, J. 1992 The dimension of attractors underlying periodic turbulent Poiseuille flow. *J. Fluid Mech.* **242**, 1–29.

Kim, J. & Hussain, F. 1993 Propagation velocity of perturbations in turbulent channel flow. *Phys. Fluids* A **5**(3), 695–706.

Kraichnan, R. H. 1970 Instability in fully developed turbulence. *Phys. Fluids* **13**, 569–575.

Leith, C. E. 1971 Atmospheric predictability and two-dimensional turbulence. *J. Atmos. Sci.* **28**, 145–161.

Leith, C. E. & Kraichnan, R. H. 1972 Predictability of turbulent flows. *J. Atmos. Sci.* **29**, 1041–1058.

Lilly, D. K. 1972 Numerical simulation studies of two-dimensional turbulence. II. Stability and predictability studies. *Geophys. Fluid Dyn.* **4**, 1–28.

Lorenz, E. 1963 Deterministic nonperiodic flow. *J. Atmos. Sci.* **20**, 130–141.

Luchini, P., Quadrio, M. & Zuccher, S. 2006 The phase-locked mean impulse response of a turbulent channel flow. *Phys. Fluids* **18**, 121702.

Lund, T. S., Wu, X. & Squires, K. D. 1998 Generation of turbulent inflow data for spatially-developing boundary layer simulations. *J. Comput. Phys.* **140**, 233–258.

Morrison, W. R. B., Bullock, K. J. & Kronauer, R. E. 1971 Experimental evidence of waves in the sublayer. *J. Fluid Mech.* **47**, 639–656.

Nikitin, N. V. 1995 Spatial approach to numerical modeling of turbulence in pipe flows. *Phys. Dokl.* **40**, 434–437.

Nikitin, N. V. 2001 Numerical analysis of laminar–turbulent transition in a circular pipe with periodic inflow perturbations. *Fluid Dyn.* **36**, 204–216.

Nikitin, N. 2006 Finite-difference method for incompressible Navier–Stokes equations in arbitrary orthogonal curvilinear coordinates *J. Comput. Phys.* **217**, 759–781.

Nikitin, N. 2007 Spatial periodicity of spatially evolving turbulent flow caused by inflow boundary conditions. *Phys. Fluids* **19**(9), 091703-4.

Orszag, S. A. & Patterson, Jr. G. S. 1972 Numerical simulation of turbulence. *Lecture Notes in Physics* vol. 12, pp. 127–147. Springer.

Rai, M. M. & Moin, P. 1993 Direct numerical simulation of transition and turbulence in a spatially evolving boundary layer *J. Comput. Phys.* **109**, 169–192.

Reynolds, W. C. & Hussain, A. K. M. F. 1972 The mechanism of an organized wave in turbulent shear flow. Part 3. Theoretical models and comparison with experiments. *J. Fluid Mech.* **54**, 263–288.

Sen, P. K. & Veeravalli, S. V. 2000*a* Hydrodynamic stability theory and wall turbulence. *Current Sci.* **79**, 840–848.

Sen, P. K. & Veeravalli, S. V. 2000*b* Behaviour of organized disturbances in fully developed turbulent channel flow. *Sadhana* **25**, 423–437.

Smagorinsky, J. 1969 Problems and promises of deterministic extended range forecasting. *Bull. Am. Met. Soc.* **50**, 286–311.

Wagner, C. & Friedrich, R. 1994 Direct numerical simulation of turbulent flow in a sudden pipe expansion. Application of direct and large eddy simulation to transition and turbulence. *AGARD-CP-551.*

Yakhot, A. Liu, H. & Nikitin, N. 2006 Turbulent flow around a wall-mounted cube: a direct numerical simulation. *Intl J. Heat Fluid Flow* **27**, 994–1009.